

Cite this: *Phys. Chem. Chem. Phys.*, 2011, **13**, 15766–15773

www.rsc.org/pccp

PAPER

Laboratory simulation of Kuiper belt object volatile ices under ionizing radiation: CO–N₂ ices as a case study†

Y. S. Kim,^a F. Zhang^a and R. I. Kaiser^{*ab}

Received 7th March 2011, Accepted 4th May 2011

DOI: 10.1039/c1cp20658c

The exposure of icy Kuiper belt objects (KBOs) by ionizing radiation was simulated in this case of exposing carbon monoxide–nitrogen (CO–N₂) ices by energetic electrons. The radiation-induced chemical processing was monitored on-line and *in situ* via FTIR spectroscopy and quadrupole mass spectrometry. Besides the array of carbon oxides being reproduced as in neat irradiated carbon monoxide (CO) ices studied previously, the radiation exposure at 10 K resulted in the formation of nitrogen-bearing species of isocyanato radical (OCN), linear (*l*-NCN), nitric oxide (NO), nitrogen dioxide (NO₂), plus diazirinone (N₂CO). The infrared assignments of these species were further confirmed by isotopic shifts. The temporal evolution of individual species was found to fit in first-order reaction schemes, prepping up the underlying non-equilibrium chemistry on the formation of OCN, *l*-NCN, and NO radicals in particular. Also unique to the binary KBO model ices and viable for the future remote detection is diazirinone (N₂CO) at 1860 cm⁻¹ (2ν₅) formed at lower radiation exposure.

1. Introduction

Since the photometric detection of a faint Kuiper belt object (1992 QB₁) beyond the orbit of Neptune, more than one thousand icy bodies of KBOs have been detected with various colors orbiting (30–50 AU) beyond Neptune of the outer solar system.^{1,2} Those solar reflection spectra in color invoked to pattern KBOs into dynamic classes of primordial origin, offering to glimpse at the era of outer solar planet formation and evolution thereafter.^{3,4} Classical KBOs, which appear visible in red for example, were named after the observation that the orbits of these meet the expectation: near-circular, less inclined and kept away from the influential Neptune's orbit.³ Within limited ranges of electromagnetic spectrum, the recent advance of ground-based spectroscopy began to unravel those chemical tracers that make up the tenuous atmospheres and surfaces of KBOs at temperatures ranging 40 to 50 K.^{5–8} Concerning retention and loss of KBO ices, it was recently computed in the framework of atmospheric escape that smaller bodies of Orcus, Charon, and Quaoar reflect off those ice features rich in water (H₂O), while larger bodies of Sedna, Eris, and Triton are still rich in volatiles of nitrogen (N₂), carbon monoxide (CO), and methane (CH₄).⁹ In the dawn of

the New Horizon spacecraft arriving to Pluto and Charon's orbits in year 2015 and some KBOs thereafter, we are about to better understand those space weathering of icy KBOs by ionizing radiation *via* detailed laboratory simulations.¹⁰ In particular, it is our current interest to gain insights into those radiation-induced effects that may cause the reddening of KBO surface layers and, in some cases, the resurfacing of pristine inner layers by the mechanism of cryovolcanism/outgassing as witnessed during the Cassini flyby to Enceladus.^{11,12}

In this case study, the radiolysis-driven chemical processing of CO–N₂ ices was simulated in the laboratory and compared to previous studies.^{13–16} In simulation of the top surface composition of Pluto and Triton, for example, premixed 1% CO in N₂ were condensed and irradiated at as low as 10 K.¹⁶ The array of CO₂, C₃O₂, N₂O, NO₂, and O₃ was commonly found in both photon- and proton-irradiated ices, plus OCN, NO, and N₃ selectively in the proton irradiated ices. Subjected to 60 keV Ar²⁺ ion irradiation, the initial CO–N₂ ices (1 : 1) were reported to yield CO₂ and C₃O₂ at a dose up to 66 eV molecule⁻¹, whereby temporal profiles of products were monitored at a decay of CO.¹⁴ Most recently, a stable complex of CO–N₂ gases known as diazirinone (N₂CO) was characterized in the gas phase *via* IR spectroscopy.¹⁷ A half-life of diazirinone was monitored about 1.5 h by the diagnostic decay of ν₁ and 2ν₅ centering at about 2040 and 1860 cm⁻¹, respectively, at room temperature. A pure form (77 K) and matrix-isolated (10 K) diazirinone were prepared as well, the latter IR spectrum of which was further corroborated in the corresponding isotopic shifts of labeled N₂CO in harmony with anharmonic calculation.^{17,18} To the best of our knowledge, these literature

^a Department of Chemistry, University of Hawaii at Manoa, Honolulu, HI 96822, USA. E-mail: ralfk@hawaii.edu

^b NASA Astrobiology Institute, University of Hawaii at Manoa, Honolulu, HI 96822, USA

† This article was submitted as part of a collection following the Low Temperature Spectroscopy/Kuiper Belt Objects symposium at Pacificchem2010.

sources have lacked, or less engaged, in conveying the comprehensive information necessary to constrain the space weathering of icy KBOs—compositions and production rates of nitrogen-bearing products, in particular. Herein, we would like to fill in this void by monitoring the interaction of CO and N₂ model ices with energetic electrons *via* dual detection schemes of a Fourier transform infrared spectroscopy (FT-IR) and quadrupole mass spectrometry during irradiation phase at 10 K and the subsequent warm-up phases.¹⁹ We also aim to provide as detailed a kinetic analysis and/or a formation mechanism of the given product so as to address the general interdisciplinary fields of readers. As a radiation source for this study, 5 keV electrons were employed to mimic secondary electrons generated in the track of MeV galactic cosmic-ray (GCR) particles penetrating the entire organic icy grains.²⁰ In this setting, a few keV μm⁻¹ of average linear energy transfer (LET) could be typically achieved mimicking those effects of MeV GCR particles on interstellar ices.

2. Experimental

The experiments were carried out in a contamination-free ultra high vacuum (UHV) stainless steel chamber as previously described.¹⁹ The UHV chamber can reach pressures down to 5×10^{-11} Torr by a magnetically suspended turbo molecular pump that is backed by a scroll pump. All pumps used are oil-free to ensure that no hydrocarbon contaminants enter the system. A polished silver mirror is suspended to the bottom of a rotary platform housed in the center of the main chamber. The silver mirror is interfaced with a two-stage closed-cycle helium refrigerator and with a programmable temperature controller to the degree that temperatures of the mirror could be regulated at a precision of ± 0.3 K between 10 K and 330 K. Gas condensation is typically carried out by the mechanism of a precision leak valve and a glass capillary array in order to linearly transfer the gas mixture to the silver substrate held at 10 K. Premixed, unlabeled gases of 45 mbar CO and 26 mbar N₂ were condensed for 8 min at a pressure of 1.0×10^{-7} torr, while isotopically labeled gases of ¹²CO–¹⁴N₂–¹⁵N₂ were premixed 13 mbar each and condensed analogously.²¹ Unless mentioned otherwise, CO–N₂ refers to the unlabeled system. Fig. 1 depicts a mid-infrared spectrum of CO–N₂ ices as deposited at 10 K. As compiled in Table 1, all but a double-hump feature at about 2050 cm⁻¹ share the band profiles and positions recorded in pure CO ices.²² The fundamental of homonuclear N₂ is not as visible at 2328 cm⁻¹ as in pure N₂ or CO₂–N₂ ices.^{23,24}

The ice sample was then irradiated isothermally with 5 keV electrons at a nominal beam current of 0 (blank) and 100 nA. The electron beams were generated with an electron gun (EQ 22/35) and aligned over a UHV phosphor screen in place of the silver mirror by scanning the sample area of 1.8 ± 0.3 cm². The actual extraction efficiency of the electron gun (Specs) was determined online using a Faraday cup to meet the stated value of 78.8%, thus correcting the fluence down to 9.8×10^{14} electrons cm⁻² hitting the target at a nominal current of 100 nA over 60 min. The radiation-induced chemical processing was then online and *in situ* monitored by a Nicolet infrared spectrometer in a spectral range of 6000 to 500 cm⁻¹.

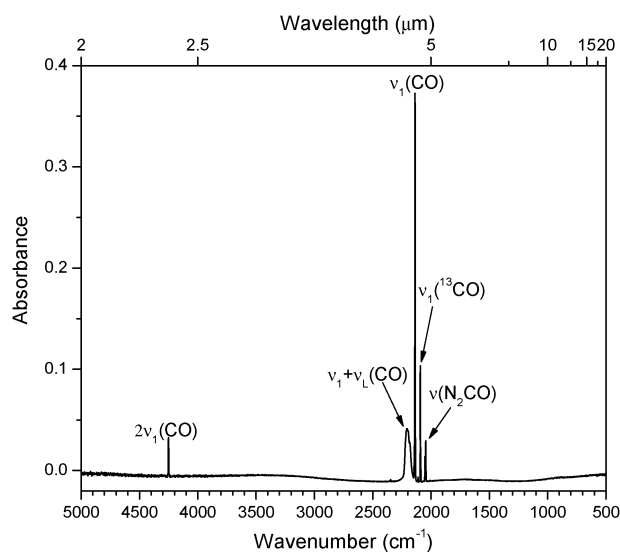


Fig. 1 Mid-infrared spectrum of carbon monoxide and nitrogen ices as deposited at 10 K. The assignments are compiled in Table 1.

Table 1 Infrared absorption features recorded before and after irradiation of carbon monoxide (CO) and nitrogen (N₂) ices at 10 K

Irradiation at 10 K		Literature assignment		
Before (cm ⁻¹)	After (cm ⁻¹)	Ref.	(cm ⁻¹)	Carrier
4251	...	22	4251	2ν ₁ (CO)
...	3708	22	3707	ν ₁ + ν ₃ (CO ₂)
...	3602	22	3602	2ν ₂ + ν ₃ (CO ₂)
...	3069	22	3070	ν ₂ + ν ₃ (C ₃ O ₂)
...	2397	22	2399	ν ₂ + ν ₄ (C ₃ O ₂)
...	2346	22	2346	ν ₃ (CO ₂)
...	2328	22	2330	ν ₃ (OC ¹⁸ O)
...	2281	22	2281	ν ₃ (¹³ CO ₂)
...	2247, 2244	22	2249, 2242	ν ₃ (C ₃ O ₂)
...	ν ₁ (C ₃ O)
~2200	...	22	~2200	ν ₁ + ν _L (CO)
...	2213	25	2212	ν ₄ (C ₅ O ₂)
...	2193	22	2194	ν ₁ (C ₃ O ₂)
2137	...	22	2136	ν ₁ (CO)
...	2123	22	2122	ν ₄ (C ₄ O ₂)
2112	...	22	2112	ν ₁ (CO–Ag)
2091	...	22	2091	ν ₁ (¹³ CO)
2088	...	22	2088	ν ₁ (C ¹⁸ O)
...	2061	25	2062	ν ₅ (C ₅ O ₂)
2051 (sh) ^a , 2046 ^a	...	17	2046	ν ₁ (N ₂ CO)
...	1987	22	1988	ν ₁ (C ₂ O)
...	1935	16	1934	ν ₃ (OCN)
...	1918	25	1919	ν ₂ (C ₄ O)
...	1912	22	1913	ν ₂ (C ₃ O)
...	1887	19	1879	2ν ₅ (CO ₃)
...	1875	16	1874	ν ₁ (NO)
...	1861 ^b	17	1860	2ν ₅ (N ₂ CO)
...	1862 ^c , 1856 ^c	27	1866	ν ₁ (NO) ₂
...	1614	24	1614	ν ₃ (NO ₂)
...	1566	22	1563	ν ₄ (C ₃ O ₂)
...	1478	26	1475	ν ₃ (NCN)
...	660	22	660	ν ₂ (CO ₂)
...	550	22	551	ν ₆ + ν _L (C ₃ O ₂)
...	541	22	542	ν ₆ (C ₃ O ₂)

Note. 60 min of irradiation (0.1 μA) of CO–N₂ ices with 5 keV electrons; Only new absorption features reported in irradiated ices at 10 K. sh: shoulder.^a Tentatively assigned. ^b Only at the lower radiation exposure. ^c Tentatively assigned, only at the higher radiation exposure.

Each spectrum was recorded in absorption-reflection-absorption mode (reflection angle $\alpha = 75^\circ$) with an integrated time of 2.5 min and a resolution of 2 cm^{-1} .¹⁹ After the irradiation is complete, the ices are kept isothermally for 60 min before being heated to 300 K with a gradient of 0.5 K min^{-1} . This allows the sublimed molecules to be detected by the quadrupole mass spectrometer (Balzer QMG 420) coupled to an electron impact ionizer, which operates in a residual gas analyzer mode a mass range of up to 200 amu.

3. Result

3.1 Infrared spectroscopy

First, we will investigate the radiation-induced formation of new species in CO–N₂ ices. Fig. 2 displays the four-panel infrared spectra of ices recorded at 10 K before (dotted trace) and after (solid trace) 60 min irradiation at 0.1 μA . The radiation exposure at 10 K leads to multiple new absorption features. A list of carriers is identified and compiled along with the vibrational assignments in Table 1.^{22,25} In fact, there were a group of absorptions which already appeared just after 2.5 min of irradiation—carbon dioxide (CO₂) at 2346 cm^{-1} , carbon suboxide (C₃O₂) at 2245 cm^{-1} , dicarbon monoxide (C₂O) at 1987 cm^{-1} , along with a carrier at 1861 cm^{-1} .^{17,22} The temporal aspect of the latter two was captured in the mid-trace of 2000–1450 cm^{-1} region (Fig. 2). Unlike the other absorptions, the feature at 1861 cm^{-1} decayed immediately, indicative of a metastable carrier—possibly diazirine ($2\nu_5$) from the ground as aforementioned earlier.¹⁷ The extent of newly formed species after 60 min of irradiation was compared with that in individually processed CO and N₂ ices (Table 1). Exclusive of some higher order species, most carbon oxide products appeared reproducibly as in irradiated CO ices;

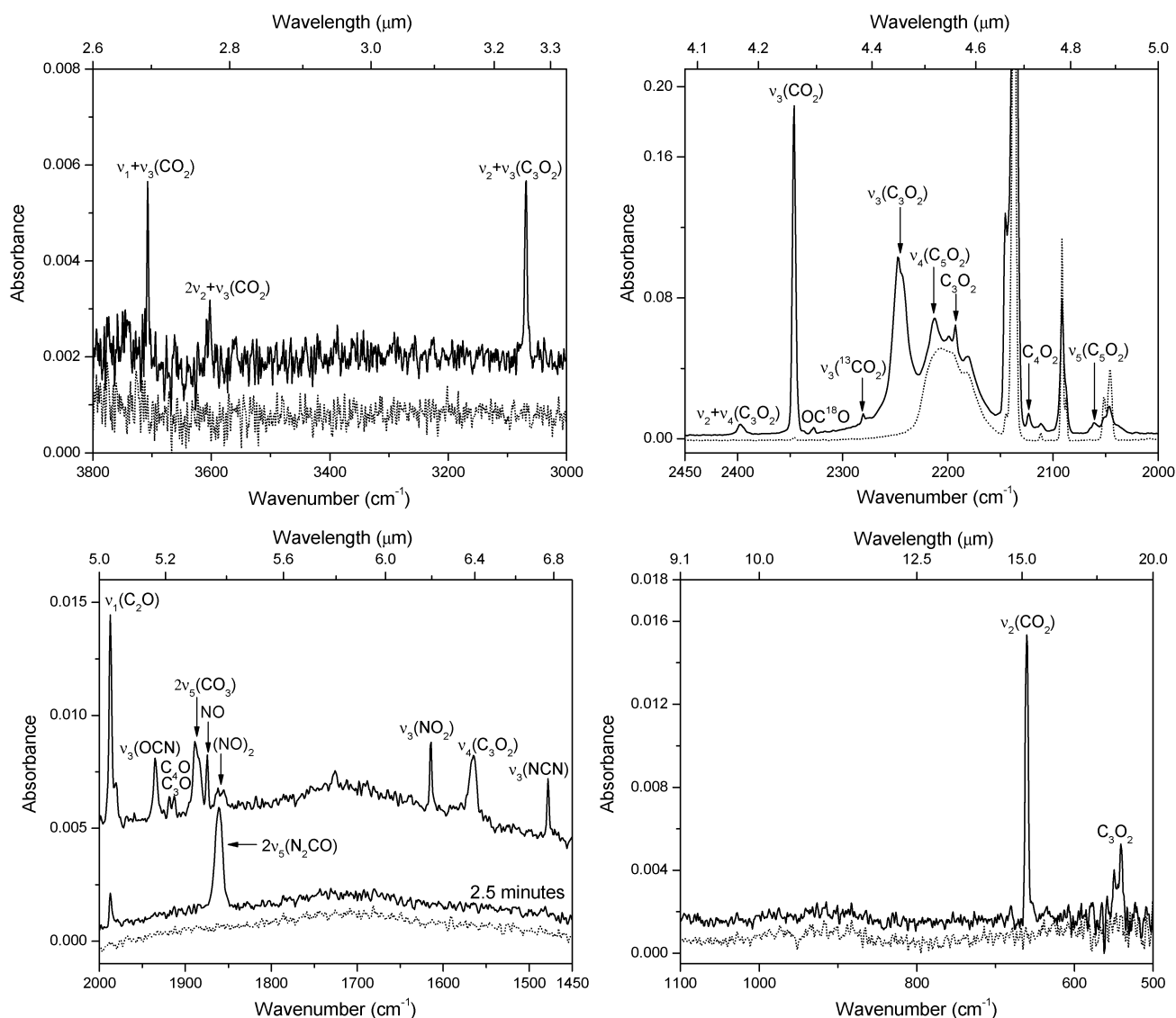


Fig. 2 Four-panel infrared spectra of carbon monoxide and nitrogen ices detailing before (dotted trace) and after (solid trace) 60 min of irradiation (100 nA) at 10 K. The carriers of newly formed features were assigned and compiled in Table 1. An extra solid trace was added in a panel of 2000–1450 cm^{-1} region in order to highlight the temporal production of diazirine ($2\nu_5$, N₂CO) and dicarbon monoxide (C₂O) just after 2.5 min of irradiation.

ozone (O_3) formation was not visible at about 1040 cm^{-1} either (Fig. 2).²² Cyclic carbon trioxide ($c\text{-CO}_3$) was evident at 1887 cm^{-1} for the Fermi-resonant $2\nu_5$ as comparable to the literature value recorded in irradiated CO_2 ice.¹⁹ No efforts were made to identify ν_1 of $c\text{-CO}_3$ at about 2040 cm^{-1} , because of the overlying feature present even before the irradiation (Fig. 1). Azide radical (N_3) was not as visible at about 1655 cm^{-1} as in irradiated N_2 ice,²³ but instead an array of nitrogen-bearing carriers appeared in the following regions: OCN at 1935 cm^{-1} (ν_3),¹⁶ NO at 1875 cm^{-1} (ν_1),¹⁶ NO_2 at 1614 cm^{-1} (ν_3),²⁴ and $l\text{-NCN}$ at 1478 cm^{-1} (ν_3).²⁶ Also tentatively assigned was a doublet feature (NO)₂ at the higher radiation exposure at about 1860 cm^{-1} , once after diazirinone ($2\nu_5$) decayed away at the lower radiation.²⁷ Note that the presence of nitrous oxide (N_2O) was not as obvious in the typical regions of about 2230 and 1290 cm^{-1} as in the irradiated ices of 1% CO in N_2 and $\text{CO}_2\text{-N}_2$.^{16,24}

Second, we will evaluate the production of those nitrogen-bearing carriers in irradiation of labeled ices. The equally mixed $^{12}\text{CO}\text{-}^{14}\text{N}_2\text{-}^{15}\text{N}_2$ were instead deposited and irradiated at 10 K. The region of $1950\text{--}1440\text{ cm}^{-1}$ was selected for comparison with the $\text{CO}\text{-N}_2$ system (Fig. 3). Clearly noticeable in irradiated $^{12}\text{CO}\text{-}^{14}\text{N}_2\text{-}^{15}\text{N}_2$ ices (upper trace) was the additional splitting(s) of each nitrogen-bearing carrier (lower trace) due to the ^{15}N substitution (Table 2). In details, OC^{14}N appears at 1934 cm^{-1} (ν_3) in the lower trace, splitting into two components in the upper trace due to the competitive formation of OC^{14}N and OC^{15}N by 7 cm^{-1} apart in frequency. The literature values of OCN isotopologues were previously recorded in vacuum ultraviolet photolysis of labeled HOCN precursors.²⁸ Despite the excellent agreement with the literature made for $2\nu_5$ of the parent diazirinone ($^{14}\text{N}_2\text{CO}$) at 1860 cm^{-1} , the agreement falls less satisfactory on the pattern of isotopic shifts.¹⁷ The band position of $^{15}\text{N}_2\text{CO}$ ($2\nu_5$) is, for example, found to deviate as much as 15 cm^{-1} from the corresponding literature value (Table 2). Provided that literature values were based on those vibrational structures in equilibrium, either computed or matrix-isolated, such deviation may then warrant further

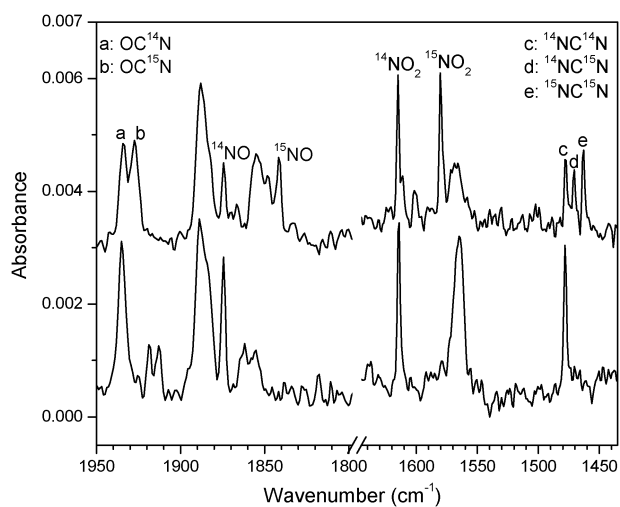


Fig. 3 Isotopic shifts of nitrogen-bearing carriers in irradiated (100 nA) $^{12}\text{CO}\text{-}^{14}\text{N}_2$ (lower trace) and $^{12}\text{CO}\text{-}^{14}\text{N}_2\text{-}^{15}\text{N}_2$ (upper trace) ices. The corresponding assignments are compiled in Table 2.

Table 2 Vibrational assignments of nitrogen-bearing carriers in irradiation of labeled $\text{CO}\text{-N}_2$ ices at 10 K

Carrier	Peak position (cm^{-1})	Literature (cm^{-1})	Ref.
$\text{O}^{12}\text{C}^{14}\text{N}$	1934	1935	28
$\text{O}^{12}\text{C}^{15}\text{N}$	1927	1928	28
$\text{O}^{13}\text{C}^{14}\text{N}$	1883	1883	28
$^{14}\text{N}_2\text{CO}$	1861	1860 ^a , 1857 ^b	17
$^{14}\text{N}^{15}\text{N}^{12}\text{CO}$...	1849 ^a , 1847 ^b	17
$^{15}\text{N}_2\text{CO}$	1852 ^c	1837 ^a , 1834 ^b	17
$^{14}\text{N}_2\text{CO}$	1809 ^c	1820 ^a , 1823 ^b	17
^{14}NO	1875	1875	27
^{15}NO	1841	1842	27
$^{14}\text{NO}_2$	1615	1618	29
$^{15}\text{NO}_2$	1580	1580	29
$^{14}\text{N}^{12}\text{C}^{14}\text{N}$	1478	1475	26
$^{14}\text{N}^{12}\text{C}^{15}\text{N}$	1471	1467	26
$^{15}\text{N}^{12}\text{C}^{15}\text{N}$	1463
$^{14}\text{N}^{13}\text{C}^{14}\text{N}$	1438	1435	26

Note. ^a Calculated frequencies ($2\nu_5$, diazirinone); ^b In Ar matrix ($2\nu_5$, diazirinone); ^c Most intense peak reported.

scrutiny on our part. On the other hand, the isotopic shifts of labeled NO_2 and NO were well reproduced relative to literature values (Table 2).^{27,29} The last species to mention is the carrier of 1478 cm^{-1} in irradiated $\text{CO}\text{-N}_2$ ices splitting into 1478 , 1471 , and 1463 cm^{-1} in $^{12}\text{CO}\text{-}^{14}\text{N}_2\text{-}^{15}\text{N}_2$ ices (Fig. 3). The temporal evolution of these bands is deconvoluted using Gaussians and fit in first-order kinetic schemes. The $l\text{-NCN}$ radical is assigned to this carrier in accord with those isotopic shifts of ν_3 to literature values (Table 2).²⁶ Note that $^{15}\text{N}^{12}\text{C}^{15}\text{N}$ at 1463 cm^{-1} in the current study was not reported in the literature matrix photolysis of labeled N_3CN .²⁶ Furthermore, irradiation of $^{13}\text{CO}\text{-}^{14}\text{N}_2$ was carried out matching the literature absorption of $^{14}\text{N}^{13}\text{C}^{14}\text{N}$ at 1438 cm^{-1} (ν_3) (Table 2).²⁶

3.2 Mass spectrometry

It is of interest to correlate the infrared observation with a mass spectroscopic analysis of the gas phase. The temporal evolution was traced at the ion currents of $m/z = 28$ (CO^+ and N_2^+), 44 (CO_2^+), and 68 (C_3O_2^+) released during warm-up phases after 0 (blank) and 100 nA irradiation of the ice mixture at 10 K (Fig. 4). Note that none of these ion currents were detected in the residual gas analyzer during the actual irradiation phase at 10 K, demonstrating that the incident electron beams did not heat or sputter the target surface. The ion current profile of $m/z = 28$ was traced for two reactants CO^+ and N_2^+ , which developed together during warm-up phases, sharing characteristics of the maximum current at about 33–34 K and the subsequent decay upward 60 K. The ion currents of $m/z = 44$ (CO_2^+) and 68 (C_3O_2^+) were also developed, just as in irradiated CO ice during warm-up phases after the processing at 10 K, peaking at about 80 K and 110 K, respectively (Fig. 4).²² Aside from diazirinone (N_2CO) being traceable in the gas phase according to the recent literature,¹⁷ any of nitrogen-bearing radical ions were not detected in the mass spectrometer, possibly due to those radicals being reactive in matrices during warm-up phases or in the gas phase before being detected in mass spectrometer.²³

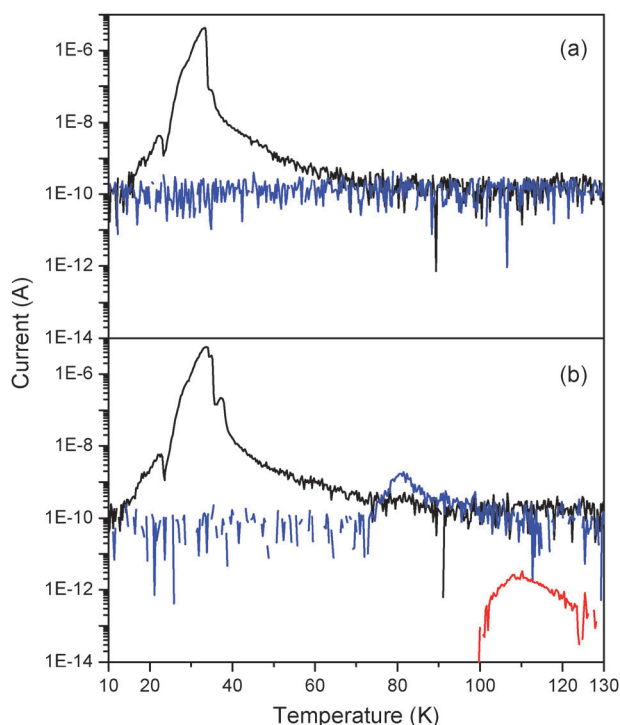


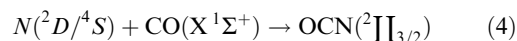
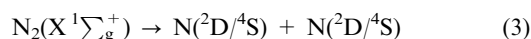
Fig. 4 Temporal evolution of the ion currents of $m/z = 28$ (CO^+ and N_2^+) in black trace, 44 (CO_2^+) in blue trace, and 68 (C_3O_2^+) in red trace during warm-up phases after the processing of CO-N_2 ices at 0 nA (A) and 100 nA (B). Traces are color-coded for clarity.

4. Discussion

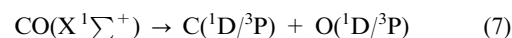
The formation of nitrogen-bearing OCN, *l*-NCN, NO, NO_2 , plus the metastable N_2CO , is currently observed in the electron-irradiated CO-N_2 ices at 10 K. This section is dedicated to gaining mechanistic insights into how these species could have formed in the simulation of KBO volatile ices under ionizing radiation, CO-N_2 ices for this case study. In utility of on-line and *in situ* FT-IR spectroscopy, the temporal (integrated IR absorption in cm^{-1}) evolution of these species, [product]_t, was monitored to fit in the first order reaction schemes of one-step (1) and consecutive $\text{A} \rightarrow \text{B} \rightarrow \text{C}$ step (2) (Fig. 5).³⁰ The rapid growth of OCN and NCN radicals was surely captured in the one-step scheme (1) of $(12.2 \pm 0.9) \times 10^{-4} \text{ s}^{-1}$ and $(3.1 \pm 0.6) \times 10^{-4} \text{ s}^{-1}$, respectively (Table 3). Based on this, one can infer non-equilibrium chemistry acting on the track of OCN and NCN formation that involves the addition of nitrogen and carbon atoms in excess energies, dissociated from N_2 and CO respectively, to the other reactant. Recall that impinging 5 keV electrons were found to induce dissociation (9.8 eV) of N_2 molecules, rendering the cleaved nitrogen atoms ($^2\text{D}/^4\text{S}$) in excess energies (3).²³ Produced in this way, electronically excited/suprathermal atoms could then react with a neighboring CO under a pseudo first-order condition to yield OCN (4); this reaction was computed to be exoergic at least by 2.4 eV.³¹

$$[\text{Product}]_t = [A]_0 (1 - e^{-kt}) \quad (1)$$

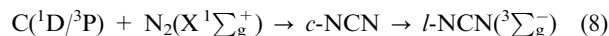
$$[\text{Product}]_t = [A]_0 \left(1 - \frac{k_2}{k_2 - k_1} e^{-k_1 t} + \frac{k_1}{k_2 - k_1} e^{-k_2 t} \right) \quad (2)$$



Likewise, carbon atoms ($^1\text{D}/^3\text{P}$) in excess energies were produced *via* two-step processes from the irradiation of CO ice at 10 K (5–6).²² The order of 8.1/6.0 eV was typically translated to the ice during the process (5) for promoting each CO molecule to the excited states ($\text{A}^1\Pi/a^3\Pi$); the excited CO then reacts back with a neighboring $\text{CO}(\text{X } ^1\Sigma^+)$ to produce $\text{CO}_2(\text{X } ^1\Sigma_g^+)$ plus a carbon atom ($^1\text{D}/^3\text{P}$).²² Note that a one-step dissociation (7) was also found to be operating in matrices.³²



Two competitive pathways are raised for electronically excited/suprathermal carbon atoms to react in the track of *l*-NCN($^3\Sigma_g^-$) formation (8–9). The pathway (8) alone poses sufficient for the competitive formation of $^{14}\text{N}^{12}\text{C}^{14}\text{N}$ and $^{15}\text{N}^{12}\text{C}^{15}\text{N}$, albeit being short for $^{14}\text{N}^{12}\text{C}^{15}\text{N}$, as proved in the irradiation of $^{12}\text{CO-}^{14}\text{N}_2\text{-}^{15}\text{N}_2$ ices (Fig. 3). On the other hand, if the pathway (9) had operated alone, the distribution of those three could have been rather statistical (1 : 2 : 1).



The stepwise pathway (8) connects to the field of combustion chemistry, where NCN is known for inducing the prompt NO formation in hydrocarbon flames.^{33–35} The reaction energetics (8) was computed to proceed *via* an intermediate of cyclic (*c*-NCN) isomer along the ground potential energy surface, overall being exoergic by 2.6 eV over an entrance barrier of 0.8 eV.³³ Cyano radicals (CN) (9) were not currently monitored at all in irradiated ices, letting us resort to those temporal profiles possibly to trace back the involvement of this pathway (Fig. 6). The temporal profile of $^{14}\text{N}^{12}\text{C}^{14}\text{N}$ by the irradiation of $^{12}\text{CO-}^{14}\text{N}_2\text{-}^{15}\text{N}_2$ ices was fit in almost the identical kinetic parameters, $k_1 = (3.2 \pm 0.7) \times 10^{-4} \text{ s}^{-1}$ and the initial concentration (A_0) = $(0.7 \pm 0.1) \times 10^{-2} \text{ cm}^{-1}$, to those found in $^{12}\text{CO-}^{14}\text{N}_2$ system (Table 3). Analogously fit was the $^{15}\text{N}^{12}\text{C}^{15}\text{N}$ profile at $(4.5 \pm 0.7) \times 10^{-4} \text{ s}^{-1}$. The formation of $^{14}\text{N}^{12}\text{C}^{15}\text{N}$ was also found to fit in a pseudo first-order condition at a slower rate, $(1.3 \pm 0.7) \times 10^{-4} \text{ s}^{-1}$. Accordingly, a branching ratio was estimated from this kinetics to favor the channel (8) over (9) at least by a factor of 1.5.

The formation of NO was previously reported in the proton-irradiated, but not in the photolyzed 1% CO in N_2 ices (Fig. 5).¹⁶ In the current electron-irradiation, NO is found to form at $(0.9 \pm 0.5) \times 10^{-4} \text{ s}^{-1}$, the slowest of all one-step fits, or comparably in the consecutive $\text{A} \rightarrow \text{B} \rightarrow \text{C}$ scheme (Table 3). Oxygen atoms ($^1\text{D}/^3\text{P}$) induced from the successive radiolysis of the CO_2 product (10) may encounter either $\text{N}(^2\text{D}/^4\text{S})$ (11) or *l*-NCN($^3\Sigma_g^-$) (12) in the track of $\text{NO}(^2\Pi)$ formation.^{22,34} The latter reaction (12) is elected resembling the prompt NO

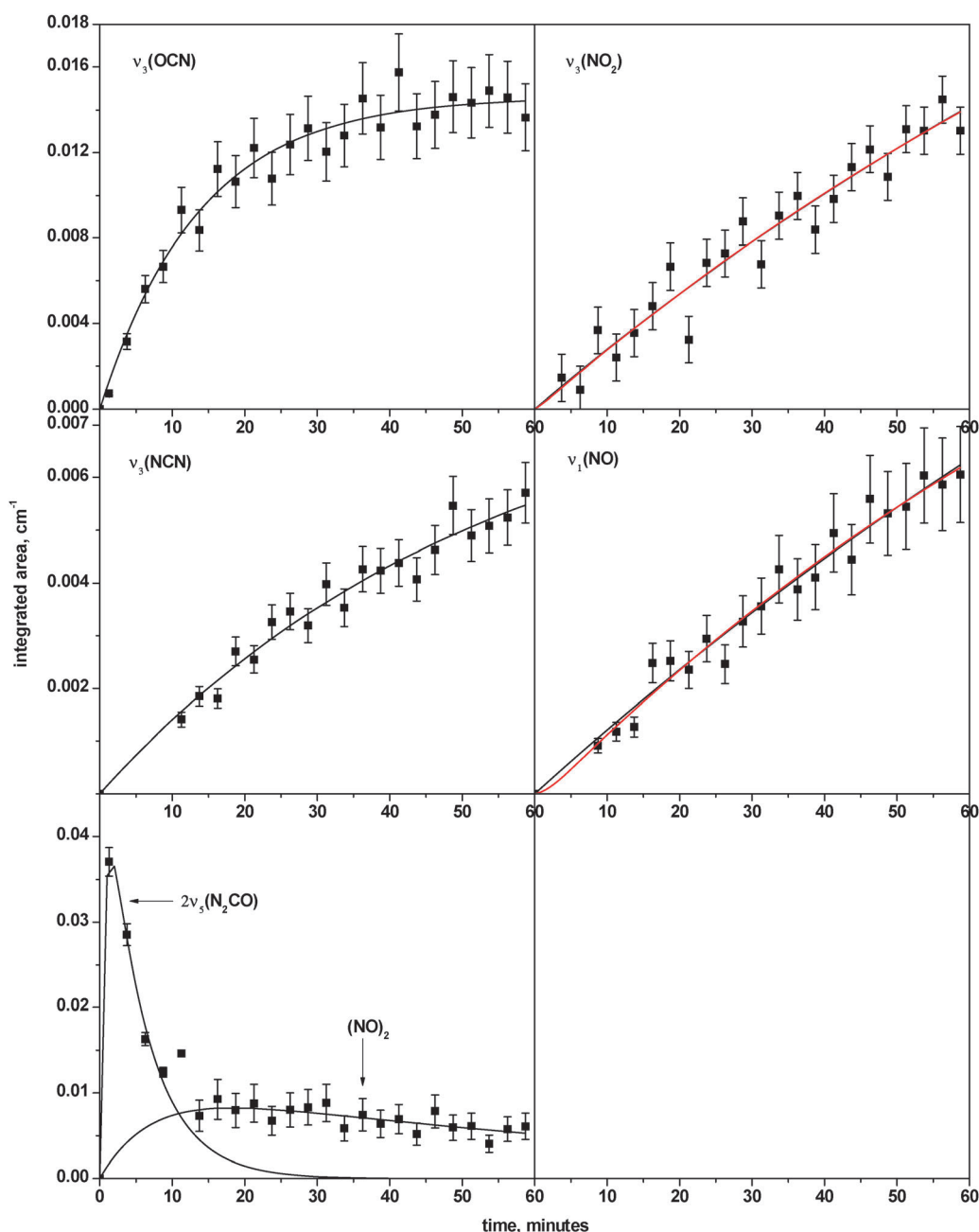
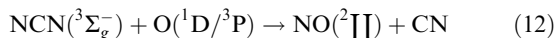
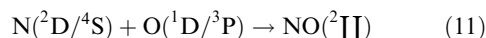
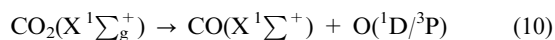


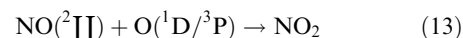
Fig. 5 Fit of temporal (integrated IR absorption) evolution of nitrogen-bearing species during radiation exposure of CO–N₂ at 100 nA. The profiles of OCN and NCN radicals are fit in one-step reaction scheme, while those of NO₂ and NO are fit and overlaid in one-step (black line) and consecutive A → B → C (red line) reaction schemes. Diazirine (N₂CO) and (NO)₂ sharing the band position at 1860 cm⁻¹ at different radiation doses are both fit for the intermediate B of A → B → C scheme; an error bar of the 5th data point is omitted for clarifying this transition.

formation in flames, possibly competing with (11) in the current ice processing.



The formation of NO₂ was previously reported together with N₂O in both photon- and proton-irradiated ices.¹⁶ In absence of N₂O from the current irradiation, NO₂ is found to form

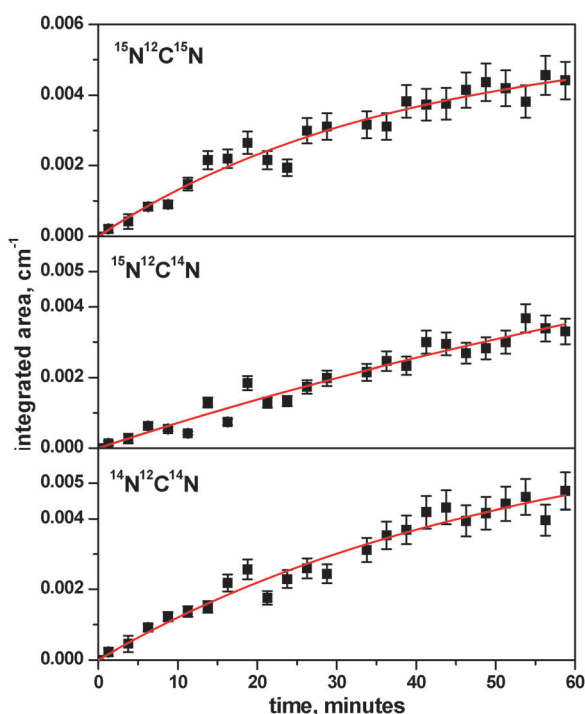
under a pseudo first order condition at $(1.1 \pm 0.8) \times 10^{-4} \text{ s}^{-1}$ (Table 3). The consumption (13) of NO is suggested to be driven by those oxygen atoms in ¹D/³P states.



The last species worthwhile mentioning is diazirine (N₂CO) at 1860 cm⁻¹ (2ν₅), the temporal profile of which was featured by the sharp rise and decay in full within the initial 15 min of irradiation (Fig. 5). It was temporally fitted for the intermediate B of consecutive A → B → C scheme, resulting in optimized rates of $k_1 = (2.7 \pm 0.7) \times 10^{-2} \text{ s}^{-1}$ and $k_2 = (0.3 \pm 0.0) \times 10^{-2} \text{ s}^{-1}$.

Table 3 Rate constants and initial concentrations derived using the first order one-step and consecutive A → B → C reaction schemes to fit the temporal evolution of nitrogen-bearing species in Fig. 5 and 6

k_1 (second ⁻¹)	k_2 (second ⁻¹)	A_0 (cm ⁻¹)	Product	Reaction scheme
¹² CO- ¹⁴ N ₂ ices at 0.1 μA				
$(12.2 \pm 0.9) \times 10^{-4}$...	$(1.5 \pm 0.0) \times 10^{-2}$	OCN	A → C
$(3.1 \pm 0.6) \times 10^{-4}$...	$(0.8 \pm 0.1) \times 10^{-2}$	NCN	A → C
$(1.1 \pm 0.8) \times 10^{-4}$...	$(4.2 \pm 2.5) \times 10^{-2}$	NO ₂	A → C
$(1.2 \pm 1.2) \times 10^{-4}$	$\sim 6.2 \times 10^{-2}$	$(3.9 \pm 3.1) \times 10^{-2}$		A → B → C
$(0.9 \pm 0.5) \times 10^{-4}$...	$(2.2 \pm 1.1) \times 10^{-2}$	NO	A → C
$(1.5 \pm 1.1) \times 10^{-4}$	$\sim 1.0 \times 10^{-2}$	$(1.5 \pm 0.8) \times 10^{-2}$		A → B → C
$(2.2 \pm 0.9) \times 10^{-4}$	$(0.2 \pm 0.1) \times 10^{-2}$	$(11.2 \pm 9.1) \times 10^{-2}$	(NO) ₂	A → B → C
$(2.7 \pm 0.7) \times 10^{-2}$	$(0.3 \pm 0.0) \times 10^{-2}$	$(5.0 \pm 0.4) \times 10^{-2}$	N ₂ CO	A → B → C
¹² CO- ¹⁴ N ₂ - ¹⁵ N ₂ ices at 0.1 μA				
$(3.2 \pm 0.7) \times 10^{-4}$...	$(0.7 \pm 0.1) \times 10^{-2}$	¹⁴ N ¹² C ¹⁴ N	A → C
$(3.2 \pm 0.7) \times 10^{-4}$	$\gg 1^a$	$(0.7 \pm 0.1) \times 10^{-2}$		A → B → C ^a
$(1.3 \pm 0.7) \times 10^{-4}$...	$(1.0 \pm 0.5) \times 10^{-2}$	¹⁴ N ¹² C ¹⁵ N	A → C
$(1.3 \pm 1.1) \times 10^{-4}$	$\sim 0.2^a$	$(1.0 \pm 0.7) \times 10^{-2}$		A → B → C ^a
$(4.5 \pm 0.7) \times 10^{-4}$...	$(0.6 \pm 0.0) \times 10^{-2}$	¹⁵ N ¹² C ¹⁵ N	A → C
$(4.5 \pm 1.1) \times 10^{-4}$	$\sim 0.4^a$	$(0.6 \pm 0.1) \times 10^{-2}$		A → B → C ^a

^a Pseudo first order.**Fig. 6** Fit of temporal (integrated IR absorption) evolution of NCN isotopologues during radiation exposure of ¹²CO-¹⁴N₂-¹⁵N₂ ices at 100 nA. Both fits of one-step (black line) and consecutive A → B → C (red line) reaction schemes are found to be indistinguishable for each case.

The following reactions (14) and (15) are suggested competing with CO₂ formation at the lower radiation exposure. That is, instead of the self-reaction with another CO (5–6), the excited CO in this binary system could find a neighboring N₂ to form the diazirinone (N₂CO) as an intermediate (B), which possibly disintegrates into CO(X¹Σ⁺) plus the excited N₂ in the course of irradiation. The diazirinone-intermediated pathway (14–15) raises further experimental investigation.



5. Conclusion

In the case study of KBO volatile ices, we irradiated CO-N₂ ices at 10 K by energetic 5 keV electrons and observed the temporal production of nitrogen-bearing species ranging OCN, *l*-NCN, NO, NO₂, plus the metastable diazirinone (N₂CO). The radiation-induced non-equilibrium chemistry was particularly evident on the temporal profiles of OCN, NCN, and NO, being fit in the decrease of pseudo first-order rates. From the irradiation of ¹²CO-¹⁴N₂-¹⁵N₂ ices, we found out two pathways competing in the formation of three NCN isotopologues. Finally, we recorded the absorption of diazirinone (N₂CO) at 1860 cm⁻¹ (2ν₅) at the lower radiation exposure in competition with CO₂ formation. Considering its thermal and radiation stabilities in gas and solid phases, we suggest that diazirinone (N₂CO) could be detectable in the future remote detection aboard a spacecraft upon approaching those KBOs.

Acknowledgements

This work was supported by the National Aeronautics Space Administration (NASA) Astrobiology Institute under Cooperative Agreement No. NNA09DA77A issued through the Office of Space Science. We would like to acknowledge Dr C. S. Jamieson (University of Hawaii) for experimental work.

References

- 1 D. Jewitt and J. Luu, *Nature*, 1993, **362**, 730–732.
- 2 <http://solarsystem.nasa.gov/planets/profile.cfm?Object = KBOs>.
- 3 S. C. Tegler, W. Romanishin and G. Consolmagno, *Astrophys. J.*, 2003, **599**, L49–L52.
- 4 <http://www.nasa.gov/topics/solarsystem/sunearthsystem/main/kuiper-colors.html>.
- 5 S. Duoté, B. Schmitt, E. Quirico, T. C. Owen, D. P. Cruikshank, C. de Bergh, T. R. Geballe and T. L. Roush, *Icarus*, 1999, **142**, 421–444.
- 6 S. C. Tegler, D. M. Cornelison, W. M. Grundy, W. Romanishin, M. R. Abernathy, M. J. Bovyn, J. A. Burt, D. E. Evans, C. K. Maleszewski, Z. Thompson and F. Vilas, *Astrophys. J.*, 2010, **725**, 1296–1305.
- 7 E. Lellouch, C. de Bergh, B. Sicardy, S. Ferron and H.-U. Käuffl, *Astron. Astrophys.*, 2010, **512**, L8.

- 8 A. Delsanti, F. Merlin, A. Guilbert-Lepoutre, J. Bauer, B. Yang and K. J. Meech, *Astron. Astrophys.*, 2010, **520**, A40.
- 9 E. L. Schaller and M. E. Brown, *Astrophys. J.*, 2007, **659**, L61–L64.
- 10 W. Zheng, D. Jewitt and R. Kaiser, *J. Phys. Chem. A*, 2009, **113**, 11174–11181.
- 11 J. Hunter Waite Jr., M. R. Combi, W.-H. IP, T. E. Cravens, R. L. McNutt Jr., W. Kasprzak, R. Yelle, J. Luhmann, H. Niemann, D. Gell, B. Magee, G. Fletscher, J. Luine and W.-L. Tseng, *Science*, 2006, **311**, 1419.
- 12 J. F. Cooper, P. D. Cooper, E. C. Sittler, S. J. Sturmer and A. M. Rymer, *Planet. Space Sci.*, 2009, **57**, 1607–1620.
- 13 J. Elsila, L. J. Allamandola and S. A. Sandford, *Astrophys. J.*, 1997, **479**, 818–838.
- 14 G. Strazzulla, J. R. Brucato, M. E. Palumbo and M. A. Satorre, *Astron. Astrophys.*, 1997, **321**, 618–624.
- 15 M. E. Palumbo, G. A. Baratta, J. R. Brucato, A. C. Castorina, M. A. Satorre and G. Strazzulla, *Astron. Astrophys.*, 1998, **334**, 247–252.
- 16 M. H. Moore and R. L. Hudson, *Icarus*, 2003, **161**, 486–500.
- 17 X. Zeng, H. Beckers, H. Willner and J. F. Stanton, *Angew. Chem., Int. Ed.*, 2011, **50**, 1–5.
- 18 C. J. Shaffer, B. J. Esselman, R. J. McMahon, J. F. Stanton and R. C. Woods, *J. Org. Chem.*, 2010, **75**, 1815–1821.
- 19 C. J. Bennett, C. Jamieson, A. M. Mebel and R. I. Kaiser, *Phys. Chem. Chem. Phys.*, 2004, **6**, 735–746.
- 20 C. J. Bennett, C. S. Jamieson, Y. Osamura and R. I. Kaiser, *Astrophys. J.*, 2005, **624**, 1097–1115.
- 21 C. Jamieson, *PhD Thesis*, University of Hawaii at Manoa, 2006.
- 22 C. Jamieson, A. M. Mebel and R. I. Kaiser, *Astrophys. J. Suppl.*, 2006, **163**, 184–206.
- 23 C. Jamieson and R. I. Kaiser, *Chem. Phys. Lett.*, 2007, **440**, 98–104.
- 24 C. S. Jamieson, C. J. Bennett, A. M. Mebel and R. I. Kaiser, *Astrophys. J.*, 2005, **624**, 436–447.
- 25 A. Trottier and R. Brooks, *Astrophys. J.*, 2004, **612**, 1214–1221.
- 26 D. E. Milligan, M. E. Jacox and A. M. Bass, *J. Chem. Phys.*, 1965, **43**, 3149–3160.
- 27 L. Krim, *J. Mol. Struct.*, 1998, **471**, 267–273.
- 28 D. E. Milligan and M. E. Jacox, *J. Chem. Phys.*, 1967, **47**, 5157–5168.
- 29 <http://webbook.nist.gov/chemistry>.
- 30 C. J. Bennett and R. I. Kaiser, *Astrophys. J.*, 2005, **635**, 1362–1369.
- 31 M. S. Schuurman, S. R. Muir, W. D. Allen and H. F. Schaefer III, *J. Chem. Phys.*, 2004, **120**, 11586.
- 32 C. J. Bennett, C. S. Jamieson and R. I. Kaiser, *Phys. Chem. Chem. Phys.*, 2010, **12**, 4032–4050.
- 33 L. V. Moskaleva and M. C. Lin, *J. Phys. Chem. A*, 2001, **105**, 4156–4163.
- 34 J. A. Sutton and J. W. Fleming, *Combust. Flame*, 2008, **154**, 630–636.
- 35 A. A. Konnov, *Combust. Flame*, 2009, **156**, 2093–2105.